Online preparation of high-quality BN coatings with atomic diffusion based on carbon-free water-soluble precursor

Yiang Du, Bing Wang[✉], Yunbo Zhang, Quzhi Song, Fuwen Wang, Cheng Han, Xiaoshan Zhang, Yingde Wang[✉]

Science and Technology on Advanced Ceramic Fibers and Composites Laboratory, College of Aerospace Science and Engineering, National University of Defense Technology, Changsha 410073, China

Abstract: Efficient and environmentally friendly production of high-quality continuous fiber coatings using current preparation methods is highly challenging due to issues such as scale and batch processing restrictions, low deposition rate, high energy consumption, and utilization of multiple environmentally hazardous steps. To address these challenges, we propose a stable and efficient wet chemical deposition coating method for high-throughput online continuous preparation of boron nitride (BN) coatings on ceramic fibers under an ambient environment. Our process involves surface modification, *in-situ* wet chemical deposition, and heat treatment, and all seamlessly connecting with the ceramic fiber preparation process through continuous stretching. Hydrophilic groups were introduced via surface modification enhancing wettability of the fiber surface with impregnating solution. An *in-situ* reaction and atom migration improve uniformity and binding of the coating. As a result, outstanding impregnation and adhesion properties are achieved. A comprehensive analysis to evaluate the impact of the BN coatings was conducted, which demonstrates that the BN-coated fibers exhibit a remarkable 36% increase in tensile strength, a 133% increase in fracture toughness, and enhanced temperature resistance of up to 1600 ℃. It provides a secure and efficient platform for cost-effective production of functional and high-quality coatings through targeted surface modification and rapid stretching impregnation.

Keywords: polymer-derived ceramics; boron nitride (BN) coatings; SiC fibers; wet chemical deposition; atomic diffusion

1　Introduction

Boron nitride (BN) has good oxidation resistance, thermal shock resistance, and chemical stability [1,2]. With its low dielectric constant, BN acts as a good insulator and can enhance electromagnetic properties as a "second phase" [3–5]. These characteristics make BN highly valuable in electronic devices [4,6]. Besides, BN has many similarities with graphite, such as density [7], hexagonal lamellar structure [8], and chemical properties [9]. All these make BN excellent and preferred interface materials [10]. Numerous studies have demonstrated BN's effectiveness as interface materials for fiber-reinforced ceramic matrix composites (CMCs) in improving thermal stability [2,11–13] and mechanical properties [14–16]. Furthermore, BN exhibits self-healing capability under high-temperature conditions [17–19], thereby enhancing the materials' strain tolerance and extending its service life [20–22]. Therefore, the preparation of high-quality boron nitride coatings on continuous ceramic fibers is of significant importance.

The exfoliation of h-BN from the bulk crystal or BN powders possesses an important position for a bottom–up method in h-BN fabrication [23]. However, this method also needs to consider how to combine exfoliated h-BN uniformly and tightly with the fibers, which limits its applications in the field of continuous ceramic

fiber coating. Chemical vapor deposition (CVD) is among the techniques commonly used for fabricating BN interfaces [14,24–26]. The coatings produced through CVD exhibit desirable properties such as homogeneity, density, continuity, and strong adhesion to the substrate, resulting in superior-quality coatings [6,25,27]. However, the challenges such as process instability, low deposition rate, corrosiveness of boron and nitrogen sources, and difficulty in batch production limit the widespread application of this method [28,29]. Additionally, the low crystallinity of the BN coatings obtained via CVD poses a significant obstacle to their practical use [30,31]. This method is relatively suitable for the preparation of BN membranes for micro components in the field of microelectronics, which are used for the insulation thermal management and are not suitable for high-throughput preparation of BN coatings on continuous ceramic fibers. The wet chemical deposition exhibits a considerable promise in the synthesis of BN interfaces due to its facile process, economic viability, and ability to facilitate large-scale coating production [32,33]. Nevertheless, further improvements are needed to enhance the continuity, homogeneity, and adhesion of coatings to the substrate [26,34,35].

Presently, the primary precursors employed in wet chemical deposition processes for BN coatings include binary precursors (H_3BO_3 and $CO(NH_2)_2$), polyborazine, and polyborazane [24,33,36]. Binary precursors (H_3BO_3 and $CO(NH_2)_2$) are readily available and non-toxic. However, the issues such as raw material ratios and solution fluidity lead to uneven coating thickness, suboptimal coating quality, and susceptibility to peeling [36–38].

[✉] Corresponding authors.
E-mail: B. Wang, bingwang@nudt.edu.cn;
　　　　Y. Wang, wangyingde@nudt.edu.cn

Polyborazine exhibits high reactivity, flammability, and explosiveness, rendering it unsuitable for industrial applications [39,40]. The presence of extraneous elements in polyborazane results in low ceramic yield and poorly compacted BN coatings, necessitating special atmosphere heat treatment [41,42]. In summary, the drawbacks of the precursors used in the current wet chemical deposition processes include low ceramic yield, incomplete and easily detachable BN coatings, and complex heat treatment procedures. Therefore, further research is required to identify appropriate precursors and preparation methodologies that can generate continuous, uniform, and high-quality boron nitride coatings in large quantities.

In this study, we designed a novel route for high-throughput continuous online preparation of high-quality BN coatings on ceramic fibers. This route is based on carbon-free and water-soluble monogenic precursor poly(ammonia borane-co-borazine) (PABB) synthesized in previous work by our group and includes fiber surface modification, impregnation *in-situ* reaction deposition, and heat treatment process. PABB exhibits high ceramic yield, water solubility, superior stability, and safety. Through the introduction of hydrophilic groups on the fiber surface, we improved the wettability of the fibers with the impregnating solution. This modification allowed the impregnating solution to spread evenly on the fibers, resulting in complete and dense high-quality BN coatings. Additionally, by designing an *in-situ* reaction between the precursor and the fibers during the wet chemical deposition, we established covalent bonds between the precursor and the fibers, forming a homogeneous coating that enhances the integrity of the coating-fiber interface. A dense boron nitride coating with different thicknesses (0.1–1.2 μm) on SiC ceramic fibers was prepared. Characterization tests on mechanical properties and high-temperature resistance of BN-coated modified SiC fibers demonstrated a 36% increase in tensile strength, a 133% increase in fracture toughness, and an elevated temperature resistance from 1400 to 1600 ℃ while maintaining the fibers' weave ability. Currently, this is the highest reported increase in the tensile strength. Our results indicate that the newly developed precursor is ideal for BN coatings, enabling rapid and safe production of high-quality fiber coatings through the wet chemical deposition.

2 Experimental

2.1 Preparation of raw materials

Ammonia–borane (AB) complex (97%) was purchased from Innochem. Nitric acid (for analysis, ca. 65% solution in water) from Acros was purchased from Innochem. Third-generation SiC fibers named KD-S that were prepared by us were used in this study. The fibers did not undergo sizing. The precursor poly(ammonia borane-co-borazine) (PABB) was prepared step by step using AB as raw materials. Firstly, a cyclic boron nitrogen six-membered ring was prepared by self-polymerization and cyclization of AB at 90–100 ℃, and then grafted onto AB at 50 ℃ to obtain the precursor. The solvent used in the reaction is fluorobenzene. A coating solution was prepared by dissolving the precursor PABB in a mixture of ethanol and deionized water to produce BN fiber coatings. To investigate the effect of solution concentrations on the morphology of the coating, precursor solution of different concentrations were configured, 2.5, 5, 7.5, and 10 wt%. Modified SiC fibers (mSiC) are fabricated by surface-treating SiC fibers with nitric acid solution of different concentrations of 20%–40% at room temperature, which grafts specified groups onto the fiber surface. To simulate a realistic

service environment, the coated fibers are characterized for their high-temperature resistance by holding them at the specified temperature for 2 h.

2.2 Preparation of BN coats

The impregnation of the fibers is carried out with roll-to-roll coating equipment. The entire operation can be carried out in ambient conditions because of hydroxide-resistant properties of the precursor. The ceramic fiber bundles were drawn through a surface modification bath and impregnating bath containing coating solution. Subsequently, the bundles passed a stabilization furnace (DZG-6020, SENXIN, 150–200 ℃), where the solvent was evaporated, and the coating was pre-cured. Pre-curing was done to avoid dissolving the applied coatings during the following coating cycles. Furthermore, the pre-curing process was applied to mitigate defects that may arise during the pyrolysis of the precursors, as well as prevent the occurrence of non-dense and peeling coatings. To pyrolyze the coatings, ceramic fiber bundles were drawn through a tube furnace (OTF-1400X, MTI) of 2 m in length at 800–1400 ℃. A draw speed of 1–10 m/min was chosen, and nitrogen was selected as the pyrolysis atmosphere. The unmodified and modified SiC fibers are named BN-SiC and BN-mSiC, respectively, after wet chemical deposition of BN coating.

2.3 Characterizations

Fourier transform infrared (FTIR) spectra were recorded on a PerkinElmer Frontier FTIR/(far infrared) FIR spectrometer in KBr pellets. The oxygen and nitrogen content of the researched fibers was determined by an oxygen/nitrogen analyzer (EMIA-820, Horiba). The carbon content was measured by a carbon/sulfur analyzer (EMIA-320V, Horiba). The boron content was analyzed by a chemical titration method. TGA was conducted on a NETZSCH STA 449C instrument in Ar at a heating rate of 10 ℃/min. The surface and cross section of the fibers were analyzed by a scanning electron microscope (FE-SEM SU8000, Hitachi). XRD patterns were obtained using a rotating anode XRD diffractometer (Cu Kα radiation, TTRAX III, Rigaku). The d-spacing value (d_{002}) is from the (002) peak using Bragg formula. The average stack height (L_c) of crystallites is from FWHM of the (002) peak using Scherrer formula. The tensile strength and Young's modulus were determined from failure tests at room temperature (Micro 350, Testometric) performed on 25 monofilaments with a gauge length of 25 mm. Each tensile strength and Young's modulus data point was the average of 20 monofilaments. The thermal conductivity of SiC, modified SiC (mSiC), and modified SiC with BN coated (BN-mSiC) were evaluated in N_2 by a thermal conductivity tester (TPS 2500S, Hot Disk), using 20 mm × 20 mm × 2 mm specimens. The electrical resistivity of SiC, modified SiC (mSiC), and modified SiC with BN coated (BN-mSiC) were evaluated in ambient environment using a precision multimeter (Sourcemeter 2400, Keithley) by the two-point probe method. Transmission electron microscopy (TEM) and high-resolution transmission electron microscopy (HR-TEM) with corresponding selected area electron diffraction (SAED) patterns were tested by a high resolution transmission electron microscope (Tecnai F20, FEI). The model of the spherical aberration correction transmission electron microscopy (STEM) is JEOL ARM-200F equipped with a Cs corrector, and the operating voltage is 200 kV.

3 Results and discussion

The properties of the precursor poly(ammonia borane-co-

borazine) (PABB) are depicted in Fig. 1, and it is observed as white solid powders (Fig. 1(a)). The precursor demonstrates good stability and solubility in water, reaching up to 12.5 wt%. As shown in Fig. 1(b), the element analysis (EA) of the precursor reveals that the precursor mainly contains B, N, and H elements, with carbon and oxygen content below 2 wt%. XPS analysis comparing B1s to N1s indicates that the precursor predominantly consists of B–N straight chain structures and boron and nitrogen hexameric rings [43] (Fig. 1(c)). Furthermore, further XPS analysis comparing C1s to O1s indicates that carbon and oxygen in the precursor powders mainly come from air adsorption, which validates the accuracy of the composition analysis by EA. Additionally, the FTIR spectroscopic analysis highlights the prevalence of B–N bonds, N–H bonds, and B–H bonds in the precursor, with minor amounts of B–O and O–H bonds (Fig. 1(d)) [11,15,33]. Remarkably, the ceramic yield of the precursor reaches an impressive 81.9%, marking a substantial 228% improvement compared to the ceramic yield of 35.8% of the carbon-free commercial precursor ammonia borane (Fig. 1(e)). During pyrolysis conversion to BN ceramics in an inert atmosphere, only small amounts of ammonia and borane molecules are released (Fig. 1(f)). In summary, the molecular transformation process from precursor PABB to BN during the heat treatment process is shown in Fig. 1(g) and Figs. S1 and S2 in the Electronic Supplementary Material (ESM). These findings establish the composition, structure, and properties of the precursor, providing solid foundation and immense potential for the preparation of BN coatings.

Impregnation solution with concentrations ranging from 2.5 to 10 wt% were prepared for the wet chemical deposition of the BN coatings, as shown in Fig. 2(a). SiC fibers impregnated with different concentrations were obtained by the fast-stretching impregnation process shown in Fig. 2(b). SEM images of the fiber

without surface modification are presented in Figs. 2(c₁)–2(c₅), displaying uniformly distributed particles of the consistent size on the fiber surface. Notably, the particle size increases with the increment of the impregnating solution concentration. This phenomenon can be attributed to limited wettability between the impregnating solution and the fibers. Contact angle tests have confirmed poor wettability of SiC fibers, which is greater than 90° with the highest contact angle of 115° as shown in Fig. 2(d).

The observed granular morphology of the coating is primarily influenced by the high surface energy of the solid–liquid contact surface and the tendency of the liquid to shrink and agglomerate. During the evaporation of the impregnating liquid, the weakening influence of gravity leads to the solution on the fiber surface aggregating and contracting into small water droplets rather than spreading out uniformly. Consequently, when the solvent evaporates and dries, BN particles are left behind. This coating morphology holds potential for further exploration in areas such as super hydrophobicity and de-icing [44,45]. Therefore, to achieve a uniform and dense BN coating, enhancing the wettability of the fibers via surface modification becomes imperative.

By the surface modification with 30% nitric acid solution at room temperature, an appropriate amount of carboxyl and hydroxyl groups were grafted onto the surface without damaging the properties of the SiC fiber itself (Figs. 3(a) and 3(d)). While the 20% nitric acid solution failed to graft the modified groups, and 30% and 40% nitric acid successfully grafted the carboxyl and hydroxyl groups on SiC fibers (Fig. 3(b)). Through the incorporation of hydrophilic groups on the surface of the SiC fibers, the wettability of the fibers is enhanced. The presence of hydroxyl and carboxyl (Fig. 3(c)) facilitates non-covalent interactions, such as van der Waals forces and hydrogen bonding, between the hydrophilic groups and the impregnating solution.
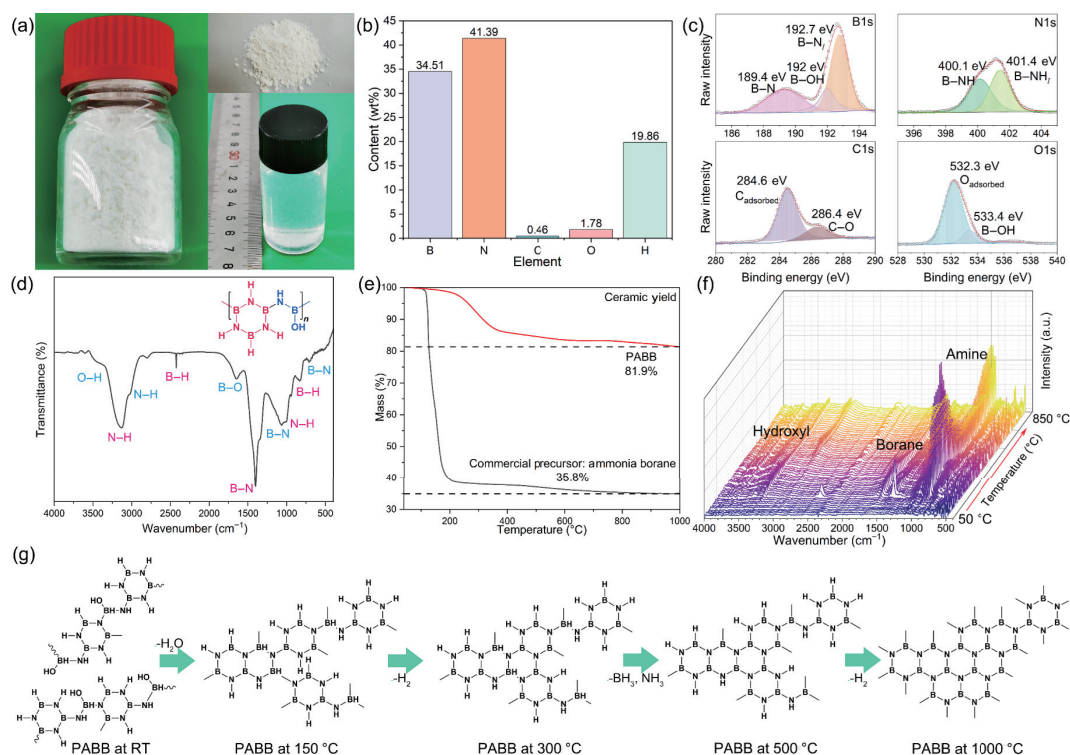

Fig. 1 Structure and properties of precursor PABB: (a) photograph of precursor PABB and its aqueous solutions. (b) Element content of precursor PABB. (c) XPS spectra of precursor PABB. (d) FTIR spectra of precursor PABB. (e) Ceramic yield of precursor PABB compared with commercial precursor ammonia borane (AB). (f) FTIR spectra of small molecules released during the pyrolysis. (g) Molecular transformation process from PABB precursor to BN during heat treatment where RT refers to room temperature.

These interactions contribute to the improved wettability of the fibers with the impregnating solution. Additionally, as illustrated in Fig. 3(c), *in-situ* reactions occur between the precursors PABB and the modified groups during the impregnation process. These reactions lead to the formation of covalent bonds, effectively grafting a substantial number of precursors directly onto the fibers with a chemical connection. This further enhances the uniformity and adhesion of the precursor impregnation. However, 40% nitric acid excessively damaged the SiC fiber mechanical properties as depicted in Fig. 3(d). Contact angle tests conducted on the modified SiC (mSiC) fibers with 30% nitric acid demonstrate a significant enhancement in wettability, with the contact angle reduced to 20°, as shown in Fig. 3(e). Therefore, we chose 30% nitric acid for hydrophilic modification.

SEM characterization of fibers impregnated at various concentrations of the impregnating solution reveals that the surface of the fibers, after being modified with hydrophilic groups, exhibits uniform and complete coating. In comparison to the scattered particles observed without surface modification, the fiber surface displays a dense coating. The SEM inset illustrates that as the concentration of the impregnating solution increases, the

density of the coating on the fiber surface gradually improves. At a concentration of 2.5 wt%, the coating surface appears rough and exhibits slight cracking, along with more pore defects (Fig. 4(a)). As the concentration reaches 5 wt%, the coating maintains its rough texture but becomes denser, resulting in the disappearance of pore defects and cracking (Fig. 4(b)). When the impregnating solution concentration exceeds 7.5 wt%, the coating surface becomes smooth and dense, with only a few particulate impurities present (Figs. 4(c) and 4(d)).

In summary, the innovative PABB-based rapid stretch impregnation process effectively produces a uniform and dense coating on the surface of the modified SiC fibers.

Further SEM analysis of the fiber cross section confirms that the coating thickness increases with the concentration of the impregnating solution (Figs. 5(a)–5(d)). This implies that the coating thickness can be precisely controlled by adjusting the impregnating solution concentration. To determine the average coating thickness, 20 fiber cross-sections impregnated at each concentration were examined, and the values were averaged. The results indicate that the coating thickness can be regulated within the range of 0.1–1.2 μm from Figs. 5(a)–5(d). Therefore, BN
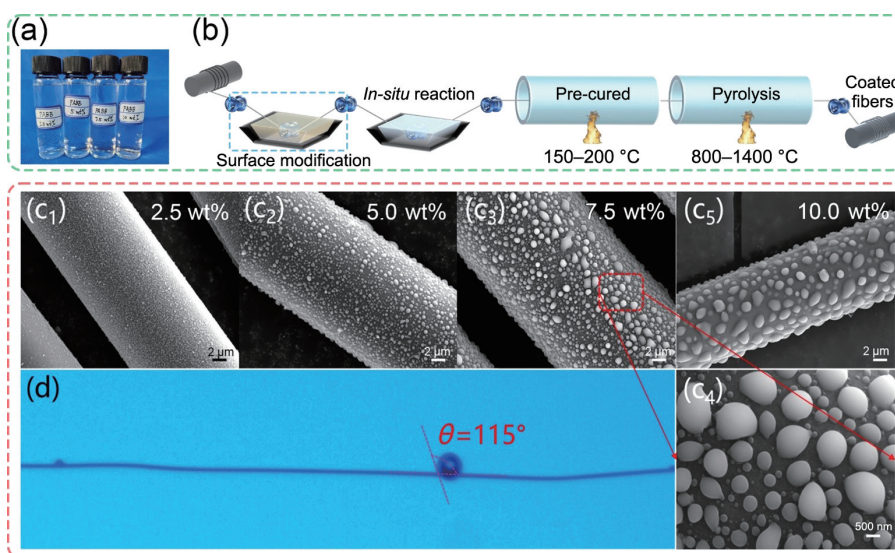

Fig. 2 Fabrication flow to achieve fast coated BN-SiC fibers: (a) coating solution of different concentrations: 2.5, 5, 7.5, 10 wt%. (b) Fabrication of BN-SiC fibers via wet chemical deposition and fast continuous drawing. SEM surface of BN-SiC fibers with impregnation solution concentration: (c$_1$) 2.5 wt%, (c$_2$) 5 wt%, (c$_3$) 7.5wt%, (c$_4$) partial enlarged of (c$_3$), and (c$_5$) 10 wt%. (d) Photograph of contact angle between impregnation solution and SiC fiber.
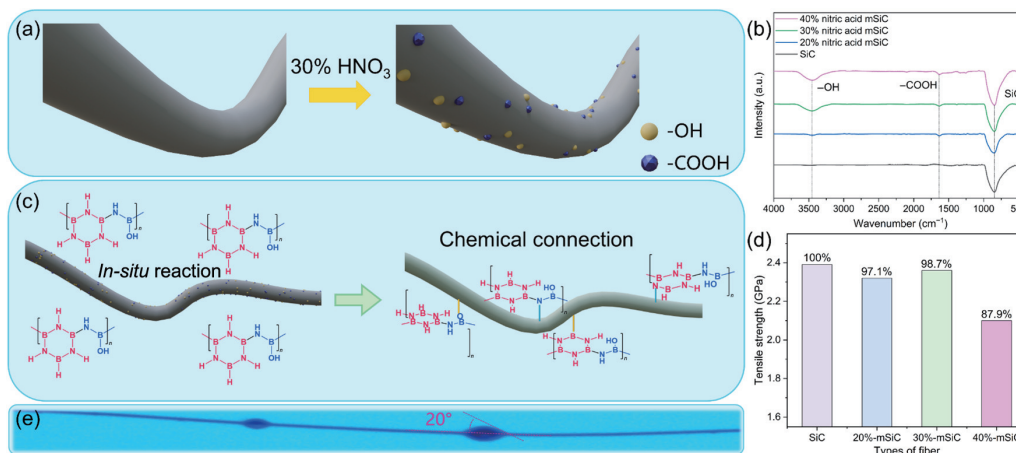

Fig. 3 Schematic diagram of fiber wettability optimization design: (a) modifing SiC fibers with hydrophilic groups; (b) FTIR spectra of SiC modified with nitric acid at different concentrations; (c) mechanism of improving wettability and wet chemical deposition uniformity of SiC fibers; (d) tensile strength of SiC modified with nitric acid at different concentrations; (e) photograph of contact angle between impregnation solution and modified SiC fiber.
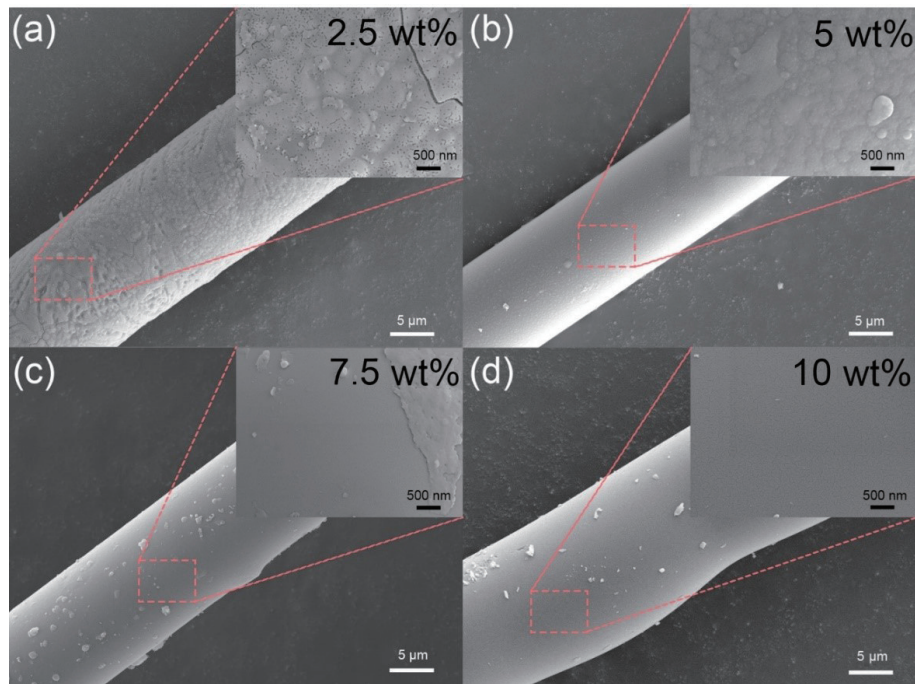
Fig. 4 SEM images of BN-mSiC fiber surfaces coated with different impregnation solution concentrations: (a) 2.5 wt%, (b) 5 wt%, (c) 7.5 wt%, and (d) 10 wt%.
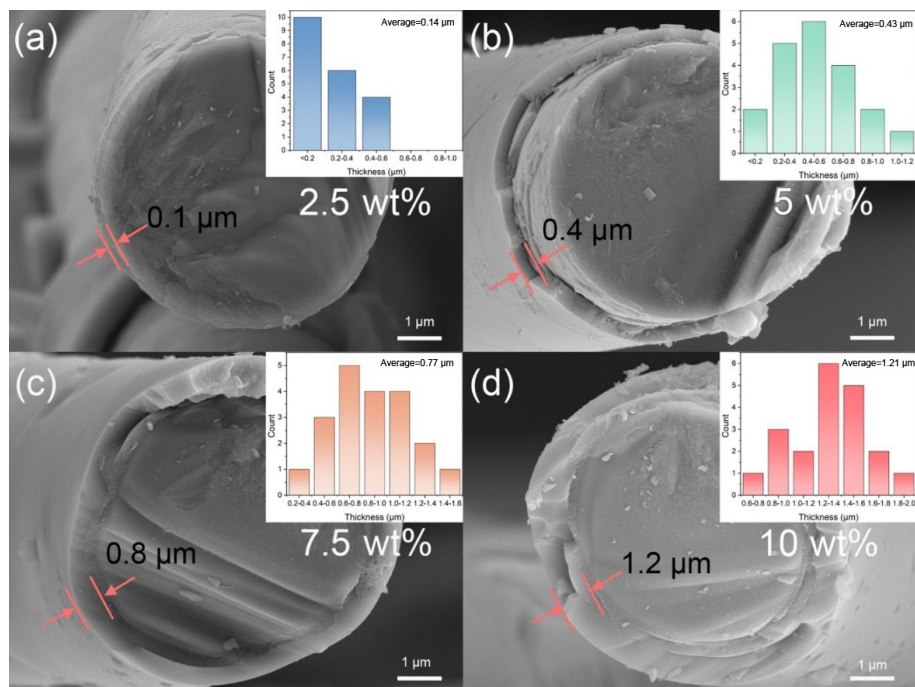

Fig. 5 SEM images of BN-mSiC fiber cross sections coated with different impregnation solution concentrations: (a) 2.5 wt%, (b) 5 wt%, (c) 7.5 wt%, and (d) 10 wt%.

coatings with different thicknesses can be prepared on the SiC fibers according to different application requirements. For example, in the interface phase application of fiber-reinforced ceramic matrix composites, a coating thickness of 0.4 μm is usually required, and a 5 wt% concentration impregnation solution can be selected. The coated fiber surfaces exhibit a dense and crack-free morphology. The coating thickness can be efficiently prepared from 0.1 up to 1.2 μm. The BN coating displays uniformity and integrity, exhibiting a close bond with the fiber without any gaps. This uniform and dense distribution can be attributed to low viscosity, high wettability of the modified fibers, and high ceramic yield of the precursor. Consequently, this process demonstrates its potential applicability to a wide range of

thicknesses for different application field.

Figure 6(a) shows modified SiC fibers coated with the BN coating (BN-mSiC). To demonstrate the composition of the fiber surface coating, the EDS analysis was conducted on the SiC fiber surface, revealing the presence of mainly B, N, and a small amount of O elements, while excluding the Si and C elements present in the fiber itself. The elements were found to be evenly distributed on the fiber surface, as depicted in Fig. 6(b) and Fig. S3 in the ESM. Furthermore, the XPS analysis was performed on the fiber surface after removing surface coating, as shown in Figs. 6(c)–6(h), to provide a comprehensive understanding of the elemental composition of the interface. The full spectral data confirmed the elemental composition of the coating. Further detailed analysis of

the narrow spectra of B and N elements revealed that the primary component of the fiber coating is boron nitride, as indicated by the binding energy of B–N bonds. Additionally, a small amount of O penetrated the coating, forming covalent bonds with B. This observation is supported by the narrow XPS spectrum of the O element. The presence of O can be attributed to two sources: the hydrophilic group introduced during fiber modification and the small amount of O element present in the precursor itself. In addition, the XPS narrow spectra of Si and C elements demonstrated the presence of covalent bonds between BN/BNO and Si/C, alongside the SiC component of the fiber itself. This finding aligns with the data obtained from the B1s XPS narrow spectrum. Consequently, the BN coating derived from the precursor not only makes a physical contact with the SiC fibers but also forms chemical bonds between the two phases through covalent bonding. This bonding mechanism elucidates why the prepared BN coatings exhibit excellent adhesion to the SiC fibers, without peeling or cracking.

Although different impregnation concentrations can be utilized to achieve a homogeneous and dense BN coating on the SiC fibers, it should be noted that these variations lead to significant differences in mechanical properties and morphology of the fibers. Figure 7(a) presents an optical photograph illustrating bending flexibility of the SiC fibers impregnated with different concentrations. It can be observed that the fibers impregnated with 5 wt% maintain their integrity without any adhesion or burrs between the fibers, even after knotting and bending. Conversely, the fibers impregnated with 10 wt% exhibit partial fractures under

the same conditions. The bending stiffness of the SiC fibers treated with different impregnation concentrations is displayed in Fig. 7(b), revealing a noticeable increase in bending stiffness above 7.5 wt% and good flexibility below 5 wt%, ensuring the fibers' weave ability. The physical properties of BN and SiC materials are completely different. BN as an electrical insulator exhibits high thermal conductivity, while SiC exhibits low thermal conductivity as a semiconductor. Therefore, the thermal conductivity and resistivity of the SiC fibers before and after the BN coating will also change accordingly. As shown in Fig. 7(c), the properties of the fibers before and after modification remain basically unchanged, indicating that the surface modification does not change the characteristics of the fibers themselves. However, after coating with BN, the thermal conductivity and electrical resistivity increase by an order of magnitude, indicating that the BN coating is continuously and uniformly coated on the fibers.

Comparative analysis of mechanical properties of the original SiC fibers, BN-coated SiC fibers (BN-SiC), and modified BN-coated SiC (BN-mSiC) fibers is presented in Figs. 8(a)–8(c) [46]. It is evident that the BN-mSiC fibers exhibit a significant advantage in terms of tensile strength and Young's modulus. The improved mechanical properties can be attributed to the more uniform and stronger bonding between the coating and the fibers after the fiber modification, resulting in greater integration between the coating and the fibers. Moreover, the coating helps reduce the stress concentration at defects within the fibers when subjected to the external stress. Compared to the original SiC fibers, the coated fibers demonstrate better retention of the mechanical strength, as
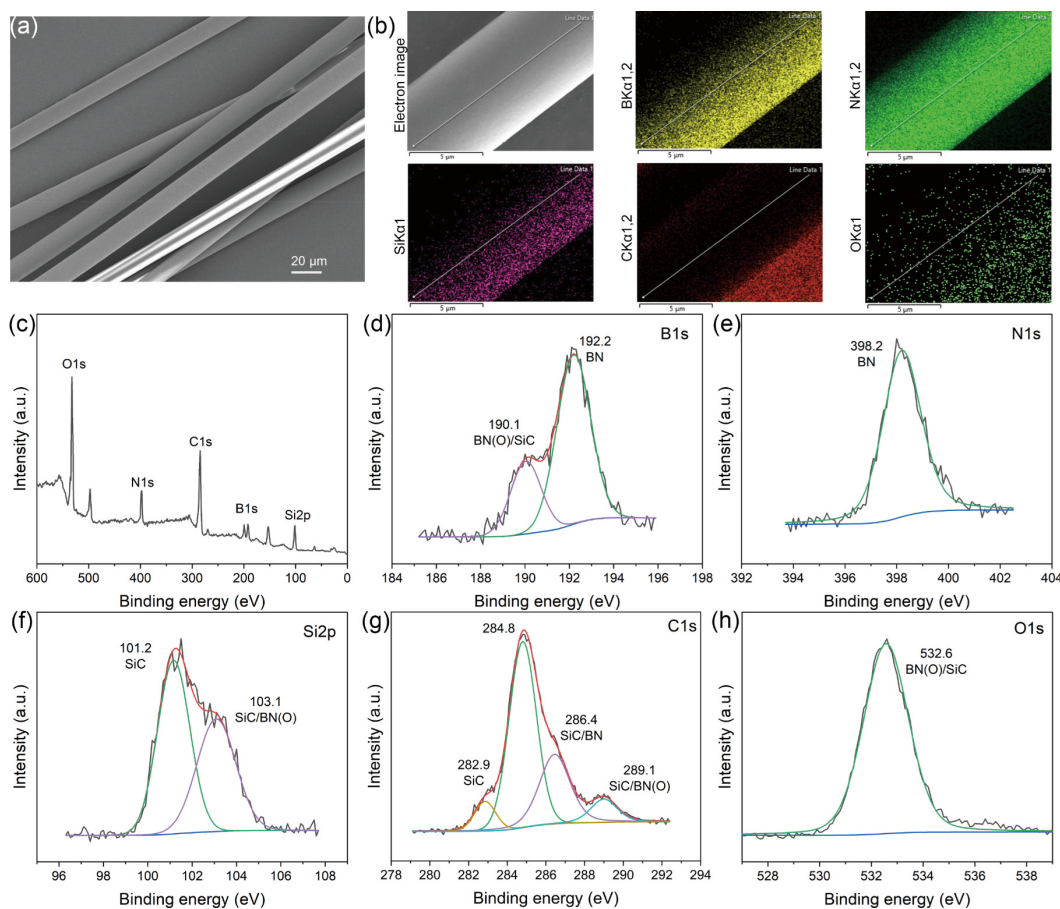

Fig. 6 Composition characterization of BN-mSiC fiber surfaces: (a) SEM images of BN-mSiC fibers with 7.5 wt% impregnation solution concentration; (b) EDS analysis of BN-mSiC fiber surfaces; (c) XPS wide spectra of BN-mSiC fiber; (d) B1s XPS spectra; (e) N1s XPS spectra; (f) Si2p XPS spectra; (g) C1s XPS spectra; (h) O1s XPS spectra of BN-mSiC fiber.
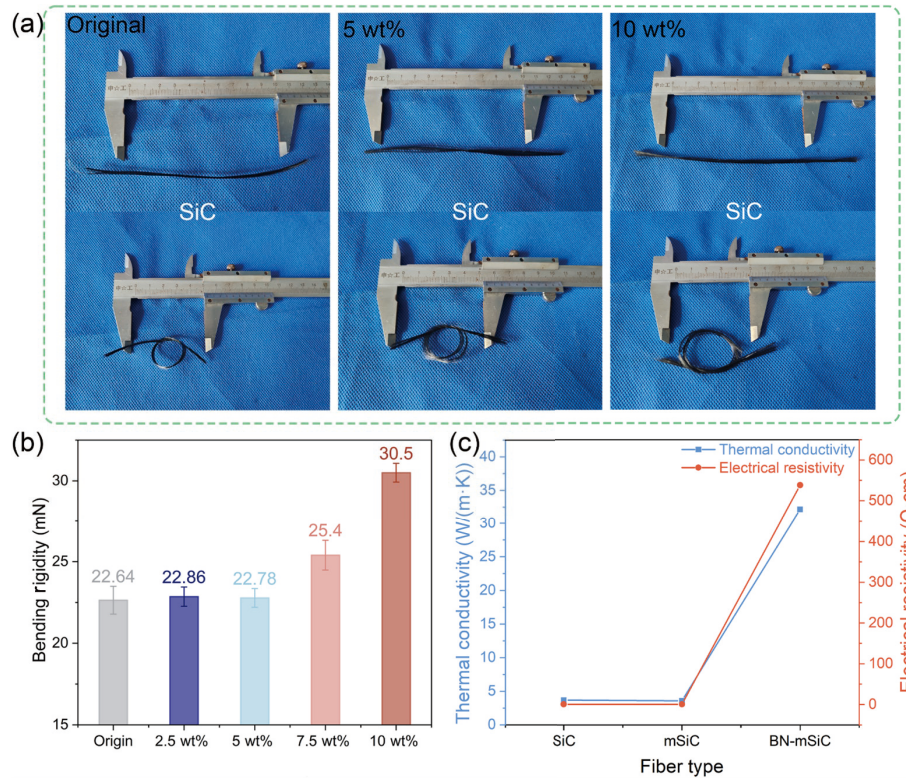
Fig. 7 Property characterization of different types of fiber: (a) photograph of BN-mSiC fibers with different impregnation concentrations; (b) BN-mSiC bundle wire bending flexibility with different impregnation concentrations; (c) thermal conductivity and electrical resistivity of fibers after different treatments.
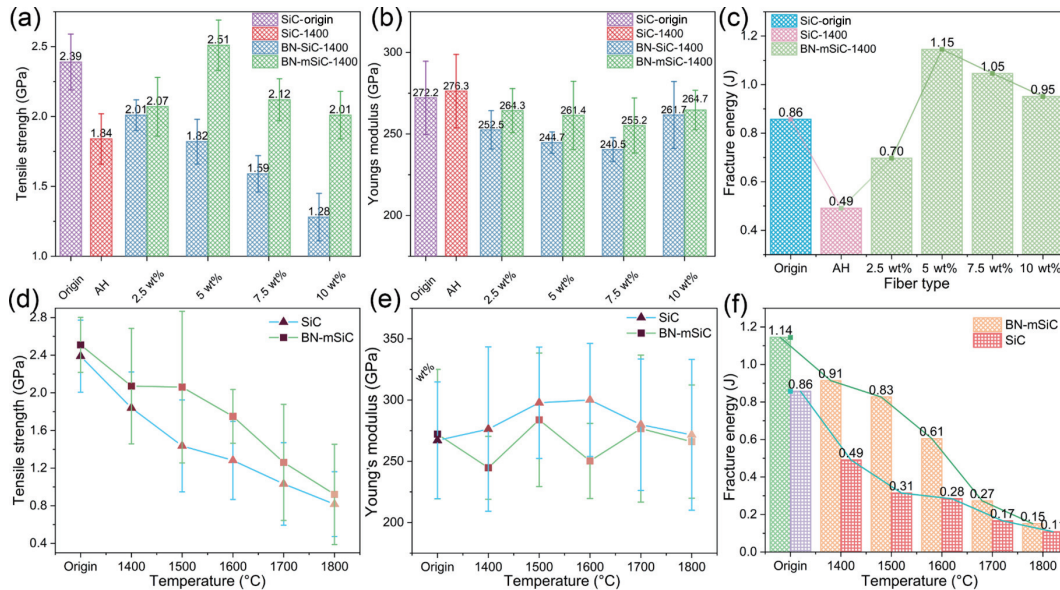

Fig. 8 Property characterization of different types of fiber: (a–c) tensile strength, Young's modulus, and fracture energy of BN-SiC and BN-mSiC fibers with different impregnation concentrations, respectively; (d–f) tensile strength, Young's modulus, and fracture energy of BN-SiC and BN-mSiC fibers after heat treatment at different temperatures, respectively.

shown in Fig. 8(a). Furthermore, the fibers impregnated with a concentration of 5 wt% exhibit a remarkable increase in the tensile strength. However, when the concentration exceeds 5 wt%, the strength slightly decreases with increasing impregnation concentration, coating thickness, and fiber diameter. Lower strength of the fibers impregnated with 2.5 wt% can be attributed to the presence of more pores and cracked defects in the coating, resulting in a less dense structure. Consequently, when subjected to external forces, the coating does not effectively disperse the forces, leading to a lack of integration with the fibers. Compared

to the SiC fibers under the same heat treatment conditions, the coated fibers exhibit a more pronounced advantage in terms of resistance to high-temperature ablation. Figure 8(c) compares the fracture energy of different fibers and demonstrates that the coating also optimizes the fracture toughness of the fibers.

Further investigation into the effect of the coating on the high-temperature resistance of the fibers is depicted in Fig. 8(d). It is evident that uncoated fibers experience a significant decrease in strength immediately after heat treatment at 1400 ℃, while the coated fibers maintain high strength even after the heat treatment

at 1600 ℃. Through TG-DSC testing (Fig. S4 in the ESM), we further verified that the high-temperature oxidation resistance of BN-mSiC is superior to that of BN SiC and SiC fibers. A significant decrease in the mechanical strength is observed for the coated fibers only after the heat treatment at 1700 ℃. Figure 7(e) shows no significant impact of heat treatment on the modulus of the fibers. Moreover, the fracture toughness of the coated fibers remains high at 1600 ℃, as illustrated in Fig. 7(f). After treatment at 1600 ℃, the fracture energy is 54% of the initial value. Consequently, the coating enables the SiC fibers to withstand higher service temperatures, increasing their threshold from 1400 to 1600 ℃.

To investigate the relationship between the microstructure of the BN coating and the macroscopic properties of the fibers, the *in situ* analysis of the coating on the fibers was performed using XRD and TEM. The XRD result depicted in Figs. 9(a) and 9(b) reveals that the BN coating on the fiber surface undergoes crystallization above 1200 ℃, exhibiting a hexagonal crystalline pattern. The (002) crystal plane spacing and domain size were estimated according to XRD patterns (Fig. 9(c)). It indicates that a heat treatment temperature of 1400 ℃ can achieve good crystallinity of h-BN, and a temperature increase of 1600 ℃ without significant increase can also cause thermal damage to the fibers. The crystalline state remains consistent across different concentrations of the impregnating solution. The TEM examination of the structure and composition of the BN coating provides further insights, as shown in Fig. 9(d). The coating is characterized by a hexagonal boron nitride lamellar structure. Notably, there is an obvious transition zone between BN and SiC phases. The EDS analysis (Fig. 9(e)) of the elemental composition confirms that the coating primarily consists of B and N, which aligns with the previous analyses. High-resolution observation reveals that the bonding between the coating and the fiber matrix is not characterized by a distinct boundary but rather a transition zone (thickness of 4–6 nm) with atomic diffusion convinced by EDS elements mappings. The XPS analysis results discussed earlier provide evidence of oxygen atoms penetrating both the BN

and SiC phases to form covalent bonds. Therefore, the transition region observed through high-resolution TEM represents the area where elements permeate each other within the two phases.

The combination between the coating and the fiber is achieved through the mutual penetration of elements, forming a strong covalent bond. This tight bond reduces the tendency for dehiscence. Figure 10 illustrates the microstructure evolution of the fiber during stretching, both before and after coating. Defects are inevitable inside and outside the fiber. During the tensile process, these defects lead to significant stress concentration. When the stress exceeds the material limit, brittle fracture occurs, particularly at the defects on the fiber surface (Fig. 10(a)). However, when the fiber surface is coated with hexagonal boron nitride, the pore defects on the fiber surface are filled with small molecules during the coating preparation. During the surface modification process of the SiC fibers, hydrophilic groups are preferentially grafted onto the micropore defects on the surface, making it easier for PABB molecules to fill the micropores via chemical bonding, reducing the impact of surface defects on fiber performance. This filling helps to release the stress at the defect under stress and alters the original fracture site and crack propagation path (Fig. 10(b)). Moreover, the *in-situ* reaction during the chemical deposition process forms a covalent bond, improving the combination of the coating and fiber, especially at micropores. Besides, it can also avoid common issues like cracking and incomplete coating. Figure 10(c) shows the atomic diffusion between the coating and the fiber surface, resulting in an atomic migration region, confirming the EDS and XPS analysis results. This atomic migration forms a transition zone between the BN crystalline phase and the SiC crystalline phase, with a thickness of approximately 4–6 nm (Fig. 10(d)). The existence of this transition zone allows the coating and fiber to be stressed together as a whole, eliminating stress concentration at the defect. Consequently, the presence of the BN coating improves the mechanical properties of fibers and prevents catastrophic failure under stress. Furthermore, the relatively dense BN coating on the SiC surface limits the silicon overflow phenomenon and restrains
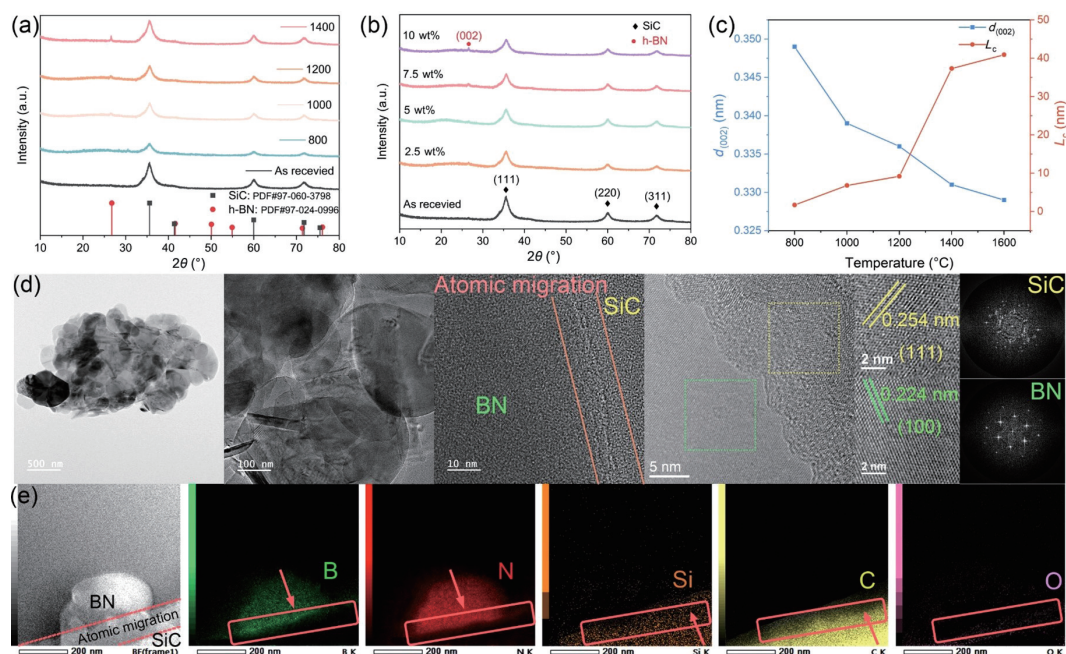

Fig. 9 Structural characterization of BN-mSiC fiber: (a) XRD patterns with different heat treatment temperatures; (b) XRD patterns with different impregnation solution concentrations; (c) crystallization analysis of BN coatings under different temperature treatments; (d) TEM images, HRTEM, and SAED of BN-mSiC fibers with 1400 ℃ heat treatment; (e) EDS analysis of BN-mSiC with 1400 ℃ heat treatment.
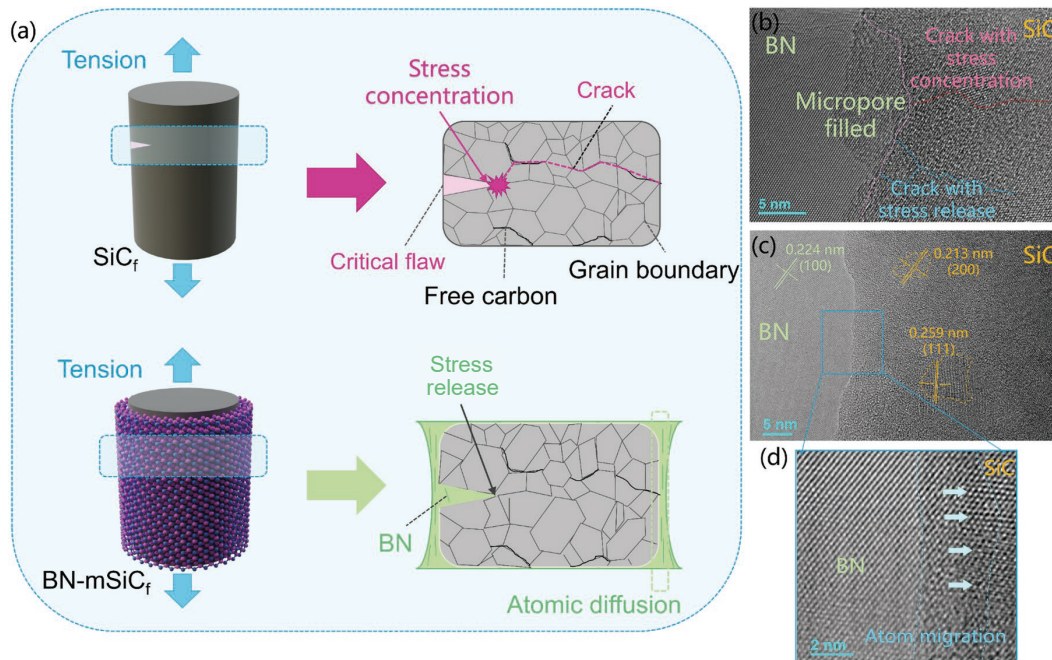
Fig. 10 Mechanism anlysis to improve strength, high-temperature resistance, and toughness of SiC fibers: (a) schematic diagram of fiber microstructure during stretching; (b) defect filling effect of BN coating; (c) atomic migration zone between BN coating and SiC fiber and (d) its enlarged image.

the growth of SiC grains at high temperatures, thereby improving the fiber's high-temperature resistance.

4 Conclusions

A novel carbon-free precursor PABB with a high ceramic yield (> 80%) which can directly transform to the high-quality dense BN coating is first reported. The favorable characteristics, including high ceramic yield, excellent stability, and superior solubility, make it an ideal choice for the wet chemical preparation of BN coatings. By utilizing this novel precursor PABB, high-quality h-BN coating with thickness and crystalline control can be more rapidly obtained via the designed method of the *in-situ* online continuous coating preparation at a low cost compared to traditional CVD methods. The high level of safety and efficiency ensure the application prospects of this method in the preparation of large components in fields such as aerospace and nuclear industry. Furthermore, based on BN coatings, the high-temperature performance of the SiC fibers has been significantly improved with a 36% increase in tensile strength, which is the highest increase in tensile strength currently reported, a 133% increase in fracture toughness, and enhanced temperature resistance of up to 1600 ℃. Building upon the analysis of the composition and structure, the atomic diffusion layer was discovered and proved to be the reason which explained the enhanced performance of the coated fibers. This is the first report on the improvement of the SiC fiber toughness based on the preparation of the BN interface phase. This work can not only achieve good bonding and thermal matching between the reinforcement and the matrix but also has the potential to further develop fiber-reinforced ceramic matrix composites.

Declaration of competing interest

The authors have no competing interests to declare that are relevant to the content of this article.

Electronic Supplementary Material

Supplementary material is available in the online version of this article at https://doi.org/10.26599/JAC.2024.9220851.

References

[1] Zheng H, Zhang WJ, Li BW, *et al*. Recent advances of interphases in carbon fiber-reinforced polymer composites: A review. *Compos Part B Eng* 2022, **233**: 109639.

[2] Christidis G, Koch U, Poloni E, *et al*. Broadband, high-temperature stable reflector for aerospace thermal radiation protection. *ACS Appl Mater Interfaces* 2020, **12**: 9925–9934.

[3] Mishra P, Saravanan P, Packirisamy G. Built in electric-field active 2D β-BN/ZIS coated water-fed photoelectrode for methane conversion into hydrogen gas and VAPs through non-oxidative coupling. *Chem Eng J* 2023, **468**: 143634.

[4] Wang JIJ, Yamoah MA, Li Q, *et al*. Hexagonal boron nitride as a low-loss dielectric for superconducting quantum circuits and qubits. *Nat Mater* 2022, **21**: 398–403.

[5] Wu ZQ, Dong J, Li XT, *et al*. Enhancing out-of-plane thermal conductivity of polyimide-based composites *via* the construction of inter-external dual heat conduction network by binary fillers. *Compos Part B Eng* 2023, **266**: 111001.

[6] Rao CNR, Gopalakrishnan K. Borocarbonitrides, $B_xC_yN_z$: Synthesis, characterization, and properties with potential applications. *ACS Appl Mater Interfaces* 2017, **9**: 19478–19494.

[7] Zhang XF, Yan PQ, Xu JK, *et al*. Methanol conversion on borocarbonitride catalysts: Identification and quantification of active sites. *Sci Adv* 2020, **6**: eaba5778.

[8] Song N, Wang P, Jin LY, *et al*. Tunable oriented cellulose/BNNSs films designed for high-performance thermal management. *Chem Eng J* 2022, **437**: 135404.

[9] Yan QW, Dai W, Gao JY, *et al*. Ultrahigh-aspect-ratio boron nitride nanosheets leading to superhigh In-plane thermal conductivity of foldable heat spreader. *ACS Nano* 2021, **15**: 6489–6498.

[10] Wang HL, Gao ST, Peng SM, *et al*. KD-S SiC$_f$/SiC composites with BN interface fabricated by polymer infiltration and pyrolysis process. *J Adv Ceram* 2018, **7**: 169–177.

[11] Huang TQ, Wang T, Jin J, *et al*. Design of silicon rubber/BN film

with high through-plane thermal conductivity and ultra-low contact resistance. *Chem Eng J* 2023, **469**: 143874.

[12] Liu JK, Feng HY, Dai JY, *et al.* A full-component recyclable Epoxy/BN thermal interface material with anisotropy high thermal conductivity and interface adaptability. *Chem Eng J* 2023, **469**: 143963.

[13] Khan A, Puttegowda M, Jagadeesh P, *et al.* Review on nitride compounds and its polymer composites: A multifunctional material. *J Mater Res Technol* 2022, **18**: 2175–2193.

[14] Chen ML, Pan L, Xia XD, *et al.* Boron nitride (BN) and BN based multiple-layer interphase for SiC$_f$/SiC composites: A review. *Ceram Int* 2022, **48**: 34107–34127.

[15] Wang F, Bai C, Chen L, *et al.* Boron nitride nanocomposites for microwave absorption: A review. *Mater Today Nano* 2021, **13**: 100108.

[16] Zhang SN, Zhong ZH, Hua Y, *et al.* Properties of super heat-resistant silicon carbide fibres with *in situ* BN coating. *J Eur Ceram Soc* 2022, **42**: 6404–6411.

[17] Lu ZL, Yue JL, Fu ZY, *et al.* Microstructure and mechanical performance of SiC$_f$/BN/SiC mini-composites oxidized at elevated temperature from ambient temperature to 1500 ℃ in air. *J Eur Ceram Soc* 2020, **40**: 2821–2827.

[18] Zheng Y, Wang SB. The effect of SiO$_2$-doped boron nitride multiple coatings on mechanical properties of quartz fibers. *Appl Surf Sci* 2012, **258**: 2901–2905.

[19] Wang SB, Zheng Y. Effect of different thickness h-BN coatings on interface shear strength of quartz fiber reinforced SiOCN composite. *Appl Surf Sci* 2014, **292**: 876–879.

[20] Teng C, Lin YC, Tan YL, *et al.* Facile assembly of a large-area BNNSs film for oxidation/corrosion-resistant coatings. *Adv Materials Inter* 2018, **5**: 1800750.

[21] Wang Z, Du LZ, Lan H, *et al.* A novel technology of sol precursor plasma spraying to obtain the ceramic matrix abradable sealing coating. *Mater Lett* 2019, **253**: 226–229.

[22] Yuan S, Toury B, Benayoun S. Novel chemical process for preparing h-BN solid lubricant coatings on titanium-based substrates for high temperature tribological applications. *Surf Coat Technol* 2015, **272**: 366–372.

[23] Tian ZB, Chen KX, Sun SY, *et al.* Crystalline boron nitride nanosheets by sonication-assisted hydrothermal exfoliation. *J Adv Ceram* 2019, **8**: 72–78.

[24] Hayat A, Sohail M, Hamdy MS, *et al.* Fabrication, characteristics, and applications of boron nitride and their composite nanomaterials. *Surf Interfaces* 2022, **29**: 101725.

[25] Luan XG, Xu XM, Li M, *et al.* Design, preparation, and properties of a boron nitride coating of silica optical fiber for high temperature sensing applications. *J Alloys Compd* 2021, **850**: 156782.

[26] Vatanpour V, Ali Naziri Mehrabani S, Keskin B, *et al.* A comprehensive review on the applications of boron nitride nanomaterials in membrane fabrication and modification. *Ind Eng Chem Res* 2021, **60**: 13391–13424.

[27] Weber M, Kim JY, Lee JH, *et al.* Highly efficient hydrogen sensors based on Pd nanoparticles supported on boron nitride coated ZnO nanowires. *J Mater Chem A* 2019, **7**: 8107–8116.

[28] Wang MQ, Jia LT, Xu HM, *et al.* Influence of pressure on chemical vapor deposition of boron nitride from BCl$_3$/NH$_3$/H$_2$ gas mixtures. *Ceram Int* 2020, **46**: 4843–4849.

[29] Yuan MJ, Zhou T, He J, *et al.* Formation of boron nitride coatings on silicon carbide fibers using trimethylborate vapor. *Appl Surf Sci* 2016, **382**: 27–33.

[30] Ye YP, Graupner U, Krüger R. Deposition of hexagonal boron nitride from N-trimethylborazine (TMB) for continuous CVD coating of SiBNC fibers. *Chem Vap Deposition* 2012, **18**: 249–255.

[31] Chen YP, Liang HW, Abbas Q, *et al.* Growth and characterization of porous sp^2-BN films with hollow spheres under hydrogen etching effect via borazane thermal CVD. *Appl Surf Sci* 2018, **452**: 314–321.

[32] Nöth A, Maier J, Schönfeld K, *et al.* Wet chemical deposition of BN, SiC and Si$_3$N$_4$ interphases on SiC fibers. *J Eur Ceram Soc* 2021, **41**: 2988–2994.

[33] Maier J, Nöth A. Wet-chemical coating of silicon carbide fibers with hexagonal boron nitride layers. *J Eur Ceram Soc* 2021, **41**: 6207–6212.

[34] Huang HW, Sheng XX, Tian YQ, *et al.* Two-dimensional nanomaterials for anticorrosive polymeric coatings: A review. *Ind Eng Chem Res* 2020, **59**: 15424–15446.

[35] Xu H, Li L, Zheng RX, *et al.* Influences of the dip-coated BN interface on mechanical behavior of PIP-SiC/SiC minicomposites. *Ceram Int* 2021, **47**: 16192–16199.

[36] Liu JG, Wang SB, Li PY, *et al.* A modified dip-coating method to prepare BN coating on SiC fiber by introducing the sol–gel process. *Surf Coat Technol* 2016, **286**: 57–63.

[37] Termoss H, Toury B, Pavan S, *et al.* Preparation of boron nitride-based coatings on metallic substrates via infrared irradiation of dip-coated polyborazylene. *J Mater Chem* 2009, **19**: 2671–2674.

[38] Zhou W, Xiao P, Li Y, *et al.* Dielectric properties of BN modified carbon fibers by dip-coating. *Ceram Int* 2013, **39**: 6569–6576.

[39] Du YA, Wang B, Li W, *et al.* Design and synthesis of a novel spinnable polyborazine precursor with high ceramic yield via one-pot copolymerization. *J Am Ceram Soc* 2021, **104**: 5509–5520.

[40] Ackley BJ, Martin KL, Key TS, *et al.* Advances in the synthesis of pre-ceramic polymers for the formation of silicon-based and ultrahigh-temperature non-oxide ceramics. *Chem Rev* 2023, **123**: 4188–4236.

[41] Song YX, Li B, Yang SW, *et al.* Ultralight boron nitride aerogels via template-assisted chemical vapor deposition. *Sci Rep* 2015, **5**: 10337.

[42] Zhang DJ, Wu FH, Ying Q, *et al.* Thickness-tunable growth of ultra-large, continuous and high-dielectric h-BN thin films. *J Mater Chem C* 2019, **7**: 1871–1879.

[43] Chen YP, Liang HW, Xia XC, *et al.* Growth temperature impact on film quality of hBN grown on Al$_2$O$_3$ using non-catalyzed borazane CVD. *J Mater Sci Mater Electron* 2017, **28**: 14341–14347.

[44] Pakdel A, Zhi CY, Bando Y, *et al.* Boron nitride nanosheet coatings with controllable water repellency. *ACS Nano* 2011, **5**: 6507–6515.

[45] Golberg D, Bando Y, Huang Y, *et al.* Boron nitride nanotubes and nanosheets. *ACS Nano* 2010, **4**: 2979–2993.

[46] Yavas D. High-temperature fracture behavior of carbon fiber reinforced PEEK composites fabricated via fused filament fabrication. *Compos Part B Eng* 2023, **266**: 110987.